

AB INITIO STUDY OF STRUCTURAL, ELECTRONIC AND OPTICAL PROPERTIES OF Al-DOPED SnO₂

M. KASHIF, T. MUNIR^{†*}, A. HUSSAIN, A. SHAHZAD, A. RASHEED,
N. AMIN, M. NOREEN, W. HUSSAIN

*Department of physics, Government College University Faisalabad (GCUF),
Allama Iqbal Road, Faisalabad 38000, Pakistan*

The structural, electronic and optical properties of pure and doped trivalent element Al(x=0, 0.0625, 0.125) in SnO₂ have been studied using full potential-linearized augmented plane wave (FP-LAPW) method based on density functional theory. The structural and electronic results indicated that as the Al concentration increases in rutile tetragonal SnO₂, lattice parameters decreases (0.01 Å and 0.02 Å and for c are 0.02 Å and 0.038 Å) and band gap increases (2.84 ~ 3.17 eV). Fermi level shift into valence band and material tends to convert into p-type semiconductor. Optical properties shows, that with increasing Al concentration in SnO₂ transparency increases and absorption spectrum has a significant blue shift. Furthermore, high static value of dielectric constant (10.5), refractive index (3.45) and low reflectivity was observed in visible region. The wide band-gap and transparent behavior for ultra-violet and visible region makes it important material for transparent applications.

(Received June 3, 2018; Accepted September 24, 2018)

Keywords: Al-doped SnO₂, Transparent conducting oxide, Low reflectivity, Band gap.

1. Introduction

Tin dioxide (SnO₂) which has become a focus of recent studies has a wide range of applications in solar cells, optoelectronic devices, flat panel display, gas sensor and catalysis. The transparent conducting oxides materials such as In₂O₃ [1], SnO₂ [2], CdO [3] and ZnO [4] develop a class of materials which shows both conductive as well as transparent behavior [5].

Tin dioxide (SnO₂) has direct band gap energy of about (3.6 eV) which makes it transparent in visible energy region and operates in ultra violet to blue wavelength. Tin dioxide (SnO₂) presents an auspicious task in short wave length LED and laser-diode because of its wide band gap (3.6 eV) and high exciton binding energy of about 130 meV[6, 7]. The higher excitation separation energy increases the luminescence efficiency of light emission.

The first principle study of pure and doped SnO₂ have been reported by many researchers [8-15] using density functional theory within LDA and GGA functional and got underestimated results as compared to experimental results. Difference of the computed energy band gaps with the experimental results illustrate that each simulation-based approximation is well-off for some oxides material up to a specific limit and accuracy but no one of these approaches is efficient in reproducing the exact experimental energy band gaps of oxides semiconductors.

DFT-based potential named modified Becke and Johnson (TB-mBJ) used to solve the problem of theoretical energy band gaps of doped oxides material [8]. This potential removes some of intrinsic drawbacks of the density functional theory [9,10]. In the present work, this exchange and correlation potential is used to reproduce the accurate band structures and optical properties of pure and doped Sn_{1-x}Al_xO₂ (x= 0, 0.0625 and 0.125).

*Corresponding author: tariqmunir@gcuf.edu.pk

2. Methodology

Fig.1 shows the unit cell of SnO₂ rutile tetragonal phase with space group of P42/mnm (No. 136) at ambient temperature and pressure. Its unit cell contains two molecules with the Sn atoms at position 2a (0,0,0) and (1/2, 1/2, 1/2) and six oxygen atoms at positions 4f (u, u,0), -(u, -u, 0), +(1/2+u, 1/2-u, 1/2) and -(1/2-u, 1/2+u,1/2).

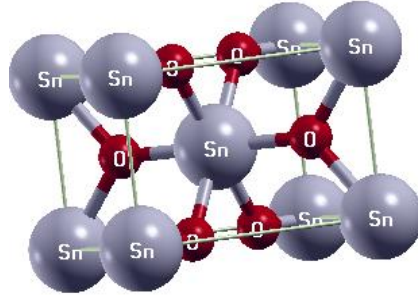


Fig.1. Rutile tetragonal structure of SnO₂.

In this present work, the full potential-linearized augmented plane wave (FP-LAPW) method used to investigate the structural, electronic and optical properties of pure and Al doped SnO₂. PBEsol-GGA exchange and correlation potential to calculate structural properties and PBE-GGA and TB-mBJ to compute electronic and optical properties within WIEN2k program based on Density Functional Theory (DFT).

3. Results

3.1. Structural properties

All calculations have been performed with Al doped 2×2×1 and 2×2×2 super-cell which contains 24 (8-Sn and 16-O) and 48 (16-Sn and 32-O) atoms respectively. The 2x2x1 and 2x2x2 doped crystal structures created by substituting one Sn atom in supercell with an aluminum atom. This corresponds to an aluminum atomic concentration at x=0.0625 and 0.125. Geometry optimization was performed for all these cases of pure and Al doped SnO₂ structures to obtain the optimized lattice parameters.

The optimized unit-cell volume can be achieved by plotting relation between volume versus total energy and after that fitted by “Birch Murnaghan equation of state” (EOS).

$$E(V) = \frac{B_0 V}{B'_0} \left[\frac{(V_0 / V)^{B'_0}}{B'_0 - 1} + 1 \right] + E_0 - \frac{V_0 B_0}{B'_0 - 1} \quad (1)$$

where,

$$B_0 = V \frac{d^2 E}{dV^2} \quad (2)$$

The lattice constant a(Å) was calculated by computing the c/a relation, next used the given formula

$$a = 0.52917706 \left(\sqrt{\frac{V_0}{c/a}} \right)^{1/3} \quad (3)$$

In equation (3), V₀ (a.b.c) possess the equilibrium volume and evaluated the “Murnaghan

equation of state". After optimization, it was observed that doped structure had the tetragonal symmetry of rutile structure. Lattice parameters and the volume of crystal structures changed by some extent. Fig.2 shows the optimization plot of pure SnO_2 .

The optimized lattice parameters are given in Table (1) are closely related to experimental values calculated by different researchers [11-19]. The computed volume decreased and lattice constants a and c also decreases as Al concentration $\text{Sn}_{1-x}\text{Al}_x\text{O}_2$ ($x=0, 0.0625, 0.125$) increases. The change in lattice parameter (\AA) is 0.01 \AA and 0.02 \AA and c is 0.02 \AA and 0.038 \AA respectively. Small change in lattice parameters is due to minor difference of ionic radii between them. The ionic radius of Al^{3+} (0.535 \AA) is smaller than that of Sn^{4+} (0.69 \AA) consequently lattice constant decreases after doping process because the lattice reduction is physically realistic [12].

Table 1. Structural properties of SnO_2 , $\text{Sn}_{1-x}\text{Al}_x\text{O}_2$ ($x=0, 0.0625, 0.125$).

Structural properties	Present results	Other calculated Results [8-15]	Experimental results
SnO_2			
a (\AA)	4.762	4.887/4.685/4.739	4.737
b (\AA)	3.233	3.283/3.156/3.161	3.186
c/a	0.678	0.672/0.673/0.667	0.673
V (\AA^3)	494.96		
$\text{Sn}_{0.9375}\text{Al}_{0.0625}\text{O}_2$			
a (\AA)	4.753	-	-
b (\AA)	3.214	-	-
c/a	0.676	-	-
V (\AA^3)	490.18		
$\text{Sn}_{0.875}\text{Al}_{0.125}\text{O}_2$			
a (\AA)	4.743	4.670	-
b (\AA)	3.196	3.142	-
c/a	0.672	0.673	-
V (\AA^3)	485.38		

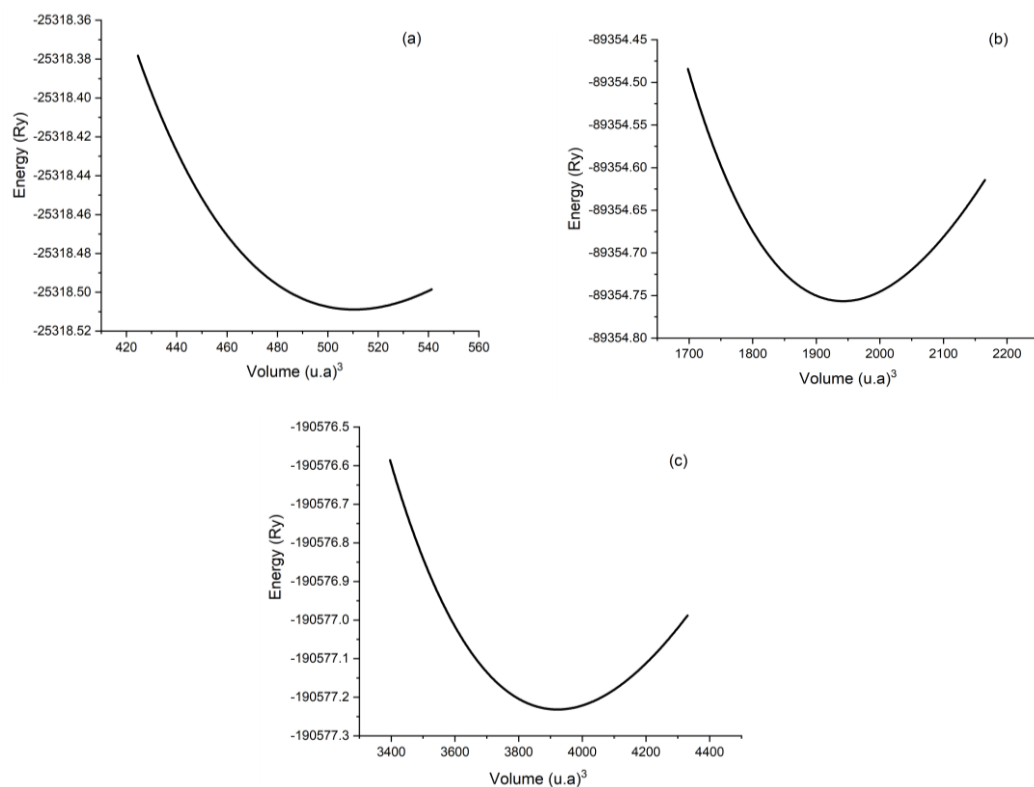


Fig. 2. Volume Optimization of (a) pure SnO_2 (b) $\text{Sn}_{0.875}\text{Al}_{0.125}\text{O}_2$ and (c) $\text{Sn}_{0.9375}\text{Al}_{0.0625}\text{O}_2$

3.2. Electronic properties

Electronic properties were obtained using GGA and TB-mBJ approximation. Fig.3 shows partial density of state (PDOS) and total density of state of pure and Al doped SnO_2 . Fig. 3(a) it is observed that upper part of valence band is mostly formed by contribution of O-2p and Sn-5p states from energy range (-7 eV to -5 eV), the O-2p state from energy range (-5eV to 0 eV) is much stronger as compared to Sn. The lowest part of conduction bands from 4eV to 7eV are essentially comprised of Sn-5s, whereas in upper part from energy range 7eV to 15eV, the 5p-Sn states more dominated to some extent by 2p-O states. The 2p-O states exhibit a hybridization nature with 5s-Sn and 5p-Sn and it is observed that valence-band is mainly originated due to Sn-5p states and O-2p states and 5s and 5p orbitals of Sn and O-2p states mainly contributed to the conduction band.

Fig.3 (b) and (c) shows the density of states of $\text{Sn}_{0.9375}\text{Al}_{0.0625}\text{O}_2$ and $\text{Sn}_{0.875}\text{Al}_{0.125}\text{O}_2$ respectively, it is observed that O- 2p states strongly hybridized with Sn- 5s, 5p and Al- 3s, 5p states in the valence band and Sn- 5p, O-2p and Al-3p states contributed to conduction band. The calculated results are in agreement with results obtained with TB-mBJ [21]. The effect of d-states of Sn atom is more as compared to O atoms of SnO_2 but the overall effect of d-state is very small [13].

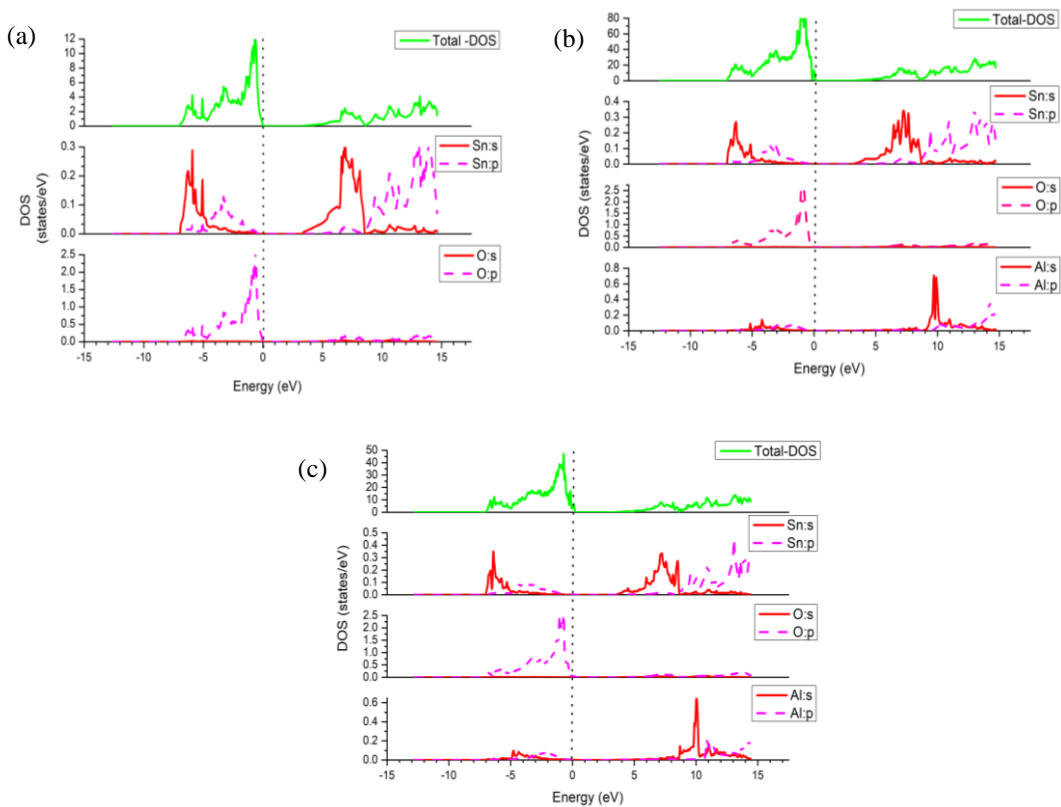


Fig. 3. Density of states of (a) pure SnO_2 (b) $\text{Sn}_{0.9375}\text{Al}_{0.0625}\text{O}_2$ (c) $\text{Sn}_{0.875}\text{Al}_{0.125}\text{O}_2$

To explore the effect on the electronic properties of the Al-doping in SnO_2 the band structure of pure and Al doped SnO_2 compared and it is observed that SnO_2 and Al-doped SnO_2 have direct band structure. The band gap calculated with the GGA approximation is 1.07eV, which is lower than the experimental value of 3.6 eV [22]. TB-mBJ approximation had been used to improve the band gap value. The band gap value of pure SnO_2 calculated by TB-mBJ approximation is 2.84 eV, which is closely to experimental and theoretical results [20, 23]. From the comparison of band structures of Al-doped SnO_2 , it was found that lower part of conduction band and upper part of valence band shift toward higher energy range and Fermi level moves toward lower energy and inserted into upper valence band which shows the dominant effect of acceptor level as shown in Fig. 4 (b) for $\text{Sn}_{0.9375}\text{Al}_{0.0625}\text{O}_2$ and in Fig.4 (c) for $\text{Sn}_{0.875}\text{Al}_{0.125}\text{O}_2$.

Therefore, Al-doped SnO_2 shows the typical p-type behavior. It is observed that Al doped SnO_2 at concentration $x = 0.125$ exhibits more p-type behavior (large band gap 3.17 eV) as compare to the pure $x = 0$ (low band gap 2.84 eV). The band gap value increases as Al concentration increases which is mainly due to smaller ionic radii of Al as compared to Sn shown in Table 2.

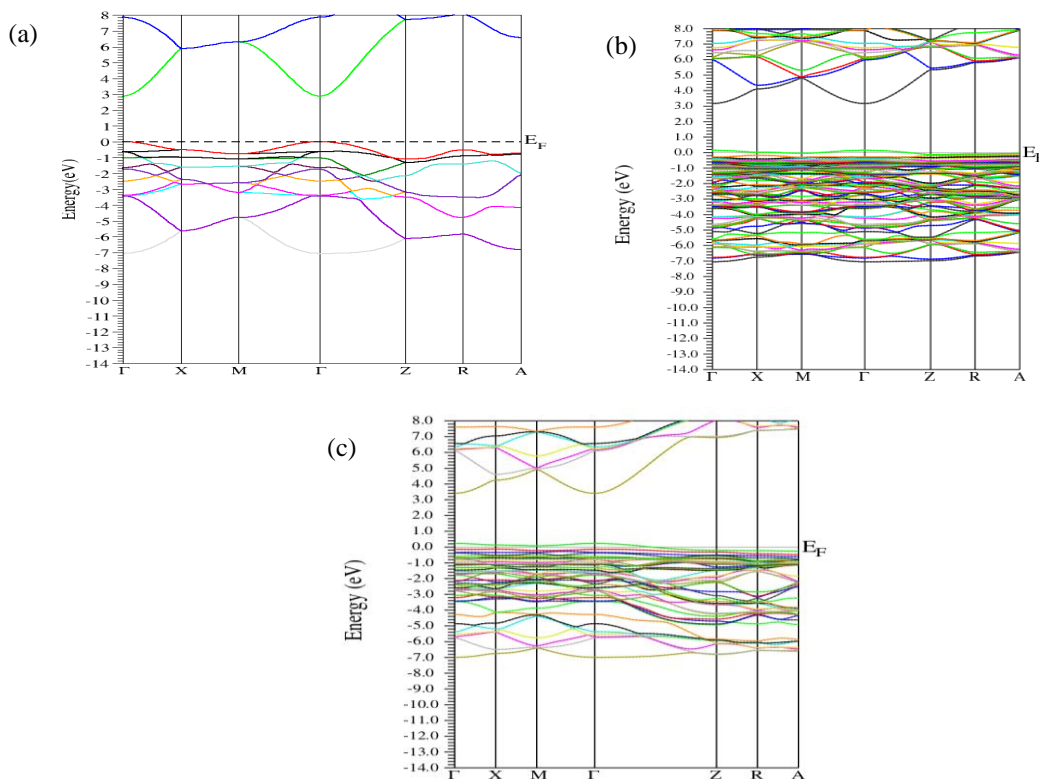


Fig. 4. Band structure of (a) pure SnO_2 (b) $\text{Sn}_{0.9375}\text{Al}_{0.0625}\text{O}_2$ (c) $\text{Sn}_{0.875}\text{Al}_{0.125}\text{O}_2$ with TB-mBJ.

Table 2. Calculated band gap with $\text{Sn}_{1-x}\text{Al}_x\text{O}_2$ ($x=0, 0.0625$ and 0.125).

Material	Present work (GGA)	Present work (TB-mBJ)	Other theoretical work
SnO_2	1.07 eV	2.84 eV	0.832/2.76 (Hassan <i>et al.</i> , 2015)
$\text{Sn}_{0.9375}\text{Al}_{0.0625}\text{O}_2$	1.18 eV	2.96 eV	-
$\text{Sn}_{0.875}\text{Al}_{0.125}\text{O}_2$	1.27 eV	3.17 eV	-

3.3. Optical properties

The optical transitions in crystal structure of solid materials are related as inter-band and intra-band transitions. Tensor components of the dielectric function $\varepsilon(\omega)$ are used to obtain the transitions. The intra-band transition does not contribute to semiconducting crystal structure but inter-band transition mainly contributed in semiconductor. The transitions are separated into two classes, first one is direct transitions and other one is indirect transitions. The indirect transitions due to photon-scattering are ignored due to negligible influence on the dielectric function $\varepsilon(\omega)$.

$$\varepsilon(\omega) = \varepsilon_1(\omega) + i\varepsilon_2(\omega) \quad (4)$$

The dielectric function $\varepsilon(\omega)$ has a frequency dependence of incident photons and separated in to real part $\varepsilon_1(\omega)$ and imaginary part $\varepsilon_2(\omega)$. The electric field of the photon leads to the optical transitions between their occupied states and unoccupied states, the imaginary part of $\varepsilon(\omega)$ is calculated from electronic structure within the joint-density of states specified by

$$\varepsilon_2 = \left(\frac{e^2 2\pi}{\Omega \epsilon_0} \right) \sum \left| \langle \psi_k^c | u \times r | \psi_k^v \rangle \right|^2 \delta(E_k^c - E_k^v - E) \quad (5)$$

Here ψ_k^c and ψ_k^v are conduction and valence band wave-function and \vec{k} and \vec{u} is the vector showing the polarization of the incident electric field and r is the position vector. The optical-constant such as reflectivity and absorption can be obtained from the dielectric-function. The real-part $\varepsilon_1(\omega)$ of dielectric function can be compute from the imaginary-part $\varepsilon_2(\omega)$ using Kramer Krong relation.

Fig.5 shows the real part $\varepsilon_1(\omega)$ of dielectric function and Fig.6 shows the imaginary part $\varepsilon_2(\omega)$ and along [100] and [001] directions of Al-doped SnO₂ at concentration ($x = 0, 0.0625, 0.125$). Fig. 5 shows that the static value of dielectric constant $\varepsilon_{(100)}$ is 2.4, 8.0 and 10.5 for pure SnO₂, Sn_{0.9375}Al_{0.0625}O₂ and Sn_{0.875}Al_{0.125}O₂ respectively along the direction [100] and for $\varepsilon_{(001)}$ is 2.65 for SnO₂ and 3.1 and 3.6 for concentration $x = 0.0625, 0.125$ respectively along the direction [001], which is closely related to experimental work [11].

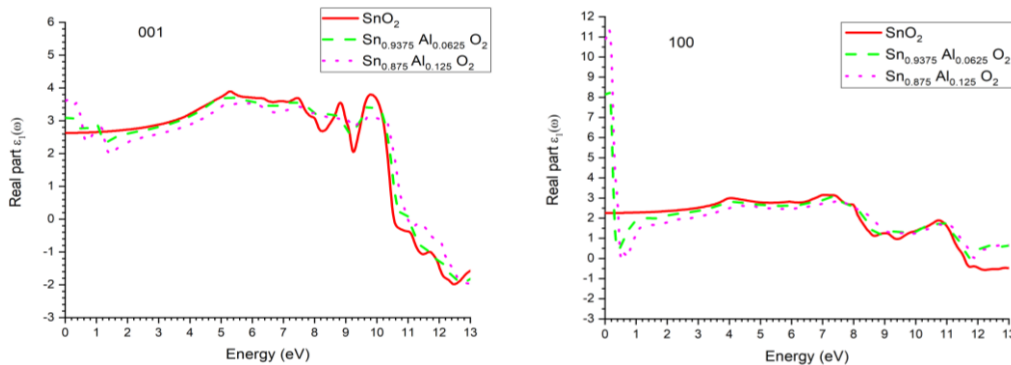


Fig. 5. Real part of $\text{Sn}_{1-x}\text{Al}_x\text{O}_2$ ($x=0, 0.0625$ and 0.125) along [100] and [001] directions

The imaginary part of dielectric function allows to determine the optically transition related valence to conduction band. With the Al-doping in SnO₂, as Al concentration increases the energy band-gap move toward higher-energy. Compared with pure SnO₂ a new small peak appeared after doping of Al in the lower energy range. These lower energy peaks mostly appear due to shifting of Fermi-level into valence band these peaks height increases as Al concentration increases. These lower energy peaks allowed to electron move from occupied state of most upper edge of valence band to un-occupied state of conduction band. After doping the first transition edge value increases as Al concentration increases and move towards the high-energy range. In near UV region as shown in Fig. 6, the peak of imaginary-part links to first transition appearing at 4.2 eV of pure SnO₂ which is consistent to the band-gap and partial density of state (PDOS) to the transition between O-2p state placed at upper edge of valence band and Sn-5s state placed at lowest edge of conduction band. The second transition happens between O-2p state from top of valence band and 5p-Sn state, the edge of this transition at near about 7.5eV, which is indicated by DOS. Other remaining peaks indicate the transition from energy range about 9 to 11eV, between 2s-O, 5s-Sn and 5p-Sn state.

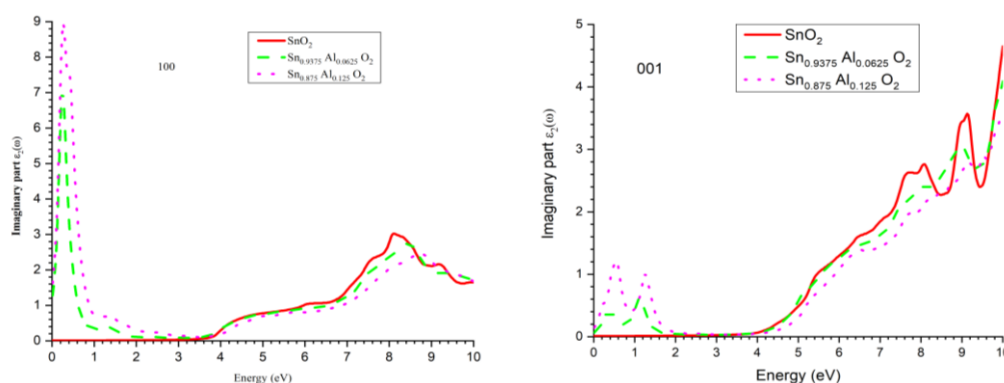


Fig. 6. Imaginary part of $\text{Sn}_{1-x}\text{Al}_x\text{O}_2$ ($x=0, 0.0625$ and 0.125) along $[100]$ and $[001]$ directions

Absorption spectra indicate that transparency is increasing as Al concentration increases shown in Fig 7. But in $[001]$ direction it shows less absorption rate as compared with $[100]$ direction. SnO_2 is an anisotropic material therefore a difference of absorption rate between these two directions is absorbed. After doping of Al a small peak appeared in the lower energy range this allowed to the electron to shift from the occupied-state of upper part of the valence to un-occupied state of conduction band. From these results, it is observed that the absorption spectrum has a significant blue shift with increasing Al concentration, which is agreement with experimental [21] and theoretical results [12].

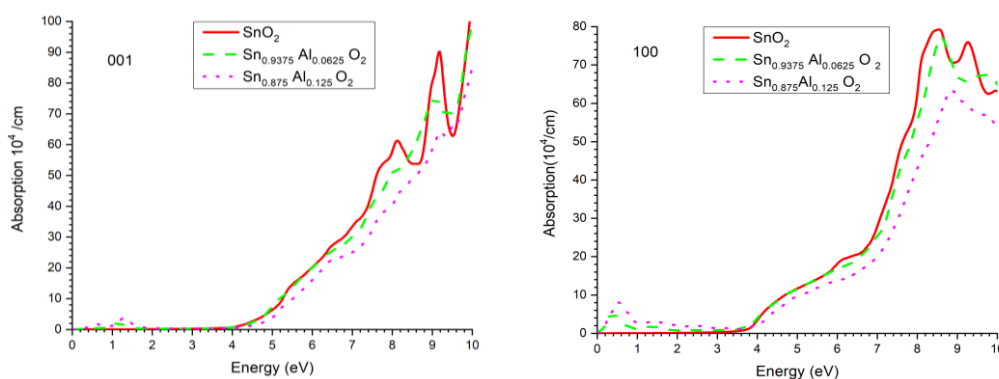


Fig. 7. Absorption of $\text{Sn}_{1-x}\text{Al}_x\text{O}_2$ ($x=0, 0.0625$ and 0.125) along $[100]$ and $[001]$ directions

Fig. 8 represents the refractive index of pure and Al doped SnO_2 along the direction $[100]$ and $[001]$. It is observed that in infrared region the speed of light propagation varies with concentration shows high interaction between incident light and other medium. From energy range (1.5 to 4 eV), the velocity of light propagation is almost equal which shows less interaction between light and medium. It was found that, a static value ($\omega = 0$) of refractive index is increases as Al concentration increases. In $[001]$ direction, the static value of refractive index of $\text{Sn}_{1-x}\text{Al}_x\text{O}_2$ at $x = 0$ is 1.63 and at $x = 0.0625, 0.125$ is 1.75 and 2.1 respectively. For $[100]$ direction, static value of refractive index of $\text{Sn}_{1-x}\text{Al}_x\text{O}_2$ at $x = 0$ is 1.58 and at $x = 0.0625, 0.125$ is 2.91 and 3.45 respectively. Refractive index value increases in $[100]$ direction as compare to $[001]$ direction therefore velocity of light in $[100]$ direction is smaller than $[001]$ direction. The static value of refractive index $n(\omega)$ of $\text{Sn}_{1-x}\text{Al}_x\text{O}_2$ enhanced by increasing Al concentration as compared to pure SnO_2 but in visible region small variation observed which is consistent with reference [14]. Fig.9 shows the low reflectivity in visible region it's about less than 20% in visible region for pure and Al doped SnO_2 along the $[100]$ and $[001]$ directions [12].

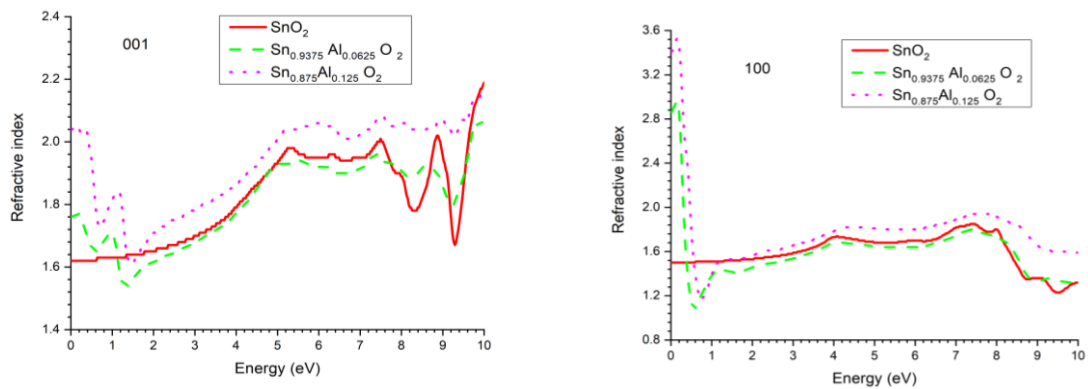


Fig. 8. Refractive index along $[100]$ and $[001]$ directions of $\text{Sn}_{1-x}\text{Al}_x\text{O}_2$ ($x = 0, 0.0625$ and 0.125).

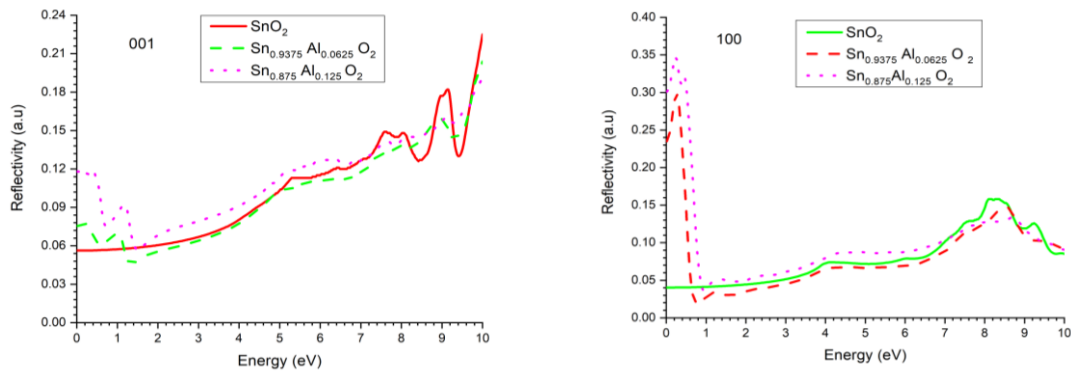


Fig.9. Reflectivity of $\text{Sn}_{1-x}\text{Al}_x\text{O}_2$ ($x = 0, 0.0625$ and 0.125) along $[100]$ and $[001]$ directions.

5. Conclusions

The structural, electronic and optical properties of pure and doped $\text{Sn}_{1-x}\text{Al}_x\text{O}_2$ at concentration ($x = 0, 0.0625$ and 0.125) were studied using FP-LAPW method. The structural and electronic results indicated that as Al concentration increases in rutile tetragonal structure SnO_2 lattice parameters decreases (0.01 \AA and 0.02 \AA and for c are 0.02 \AA and 0.038 \AA) and band gap increases ($2.84 \sim 3.17 \text{ eV}$). Fermi level shift into valence band and material tends to convert into p-type semiconductor.

The calculated density of state of Tin and Aluminum allows a sufficient description in the structure of transition of electrons. Optical transition shifted to the higher energy range, high static value of dielectric constant (10.5) and refractive index (3.45) as the Al concentration increases in SnO_2 . The optical absorption edge of SnO_2 doped with Al shows a blue shift. At $x=0.0625$ concentration of Al, it optically more transparent in visible region as compared to $x=0.125$. Furthermore, low reflectivity was observed in visible region. The wide band-gap and transparent behavior for ultra-violet and visible region makes it important material for transparent applications.

Acknowledgement

The Authors would like to acknowledge Department of Physics, Government College University Faisalabad for providing their facility.

References

- [1] H. L. Hartnagel, A. L. Dawar, A. K. Jain, C. Jagadish, (Semiconducting Transparent Thin Films Institute of Physics Publishing. Bristol, Philadelphia, PA. (1995).
- [2] P. Prathap, Subbaiah, M. Y. V. Devika, K. R. Reddy. *Mater. Chem. Phys.* **100**(2),375 (2006).
- [3] A. P. Mammana, E. S. Braga, I. Torriani, R. L. Anderson. *Thin Solid Films.* **85**(3),355 (1981).
- [4] C. Sravani, P. S. Reddy, P. J. Reddy. *Mater Lett.* **12**(6), 406 (1992).
- [5] M. Takeuchi, S. Kashimura, S. Ozawa. *Vacuum* **41**, 7 (1990).
- [6] B. Yu, C. Zhu, F. Gan. *Opt. Mater.* **7**, 15 (1997).
- [7] M. Batzill, U. Diebold. *prog. Surf.Sci.* **79**,47 (2005).
- [8] F. Tran, P. Blaha. *Phys. Rev. Lett.* **102**,22640 (2009).
- [9] P. Hohenberg, W. Kohn. *Phys. Rev. B* **136**,864 (1964).
- [10] W. Kohan, L.J. *Phys. Rev. A* **140**,1133 (1965).
- [11] Q. J. Liu, Z.T. Liu, L.P. Feng. *Comput. Mater.Sci.* **47**(4),1016 (2009).
- [12] Y. M. Liu, L. Z. Zhao, K. N. Qin, Z. Y. Cui, S. J. Li. *Mater. Res. Innovations.***18**, 522(2014).
- [13] S. Li, Z. Lu, Z. Yang, X. Chu. *Sens. Actuators, B.***202**, 83 (2014).
- [14] P. L. Fei, S. Yue, Y. Zhong-Yuan, Z. Long, L. Qiong-Yao, M. Shi-Jia, L. Yu-Min. *Commun. Theor. Phys.***57**, 145 (2012).
- [15] J. Xu, S. P. Huang, Z. S. Wang. *Solid State Commun***149**,527 (2009).
- [16] W. Z. Xiao, L. Wang, L. Xu, Q. Wan, B. S. Zou. *Solid State Commun.* **149**(31),1304 (2009).
- [17] H.J. Xu, T. Jarlborg, A.J. Freeman. *Phys. Rev. B* **40**,7939 (1989).
- [18] Z.G. Zhu, R.C. Deka, A. Chutia, R. Sahnoun, H. Tsuboi, M. Koyama, N. Hatakeyama, A. Endou, H. Takaba, A.D. Carpio, M. Kubo, A. Miyamoto. *J. Phys. Chem. Solids.* **70**,1248 (2009).
- [19] S.A. Pianaro, P.R. Bueno, P. Olivi, E. Longo, J.A. Varela. *J. Mater. Sci. Mater. Electron* **9**, 159(1998).
- [20] M.A. Bezzerrouk, M. Hassan, R. Baghdad, S. Reguieg, M. Bousmaha, B. Kharroubi. *Super lattices Microstruct.***84**,80 (2015).
- [21] S. F. Ahmed, S. Khan, P. K. Ghosh, M. K. Mitra, K. Chattopadhyay. *J. Sol-Gel Sci. Techno.* **39**(3),241 (2006).
- [22] B. Ealet, M. H. Elyakhloufi, E. Gillet, M. Ricci. *Thin Solid Films* **250**(1-2),92 (1994).
- [23] V. T. Agekyan. *Physica Status Solidi (a)*, **43**(1),11 (1977).